Fenton-like oxidation of Rhodamine B in the presence of two types of iron (II, III) oxide

Xiaofei Xue [a,b], Khalil Hanna [b,*], Nansheng Deng [a]

[a] *School of Resources and Environmental Science, Department of Environmental Science, Wuhan University, Wuhan 430079, PR China*
[b] *Laboratoire de Chimie Physique et Microbiologie pour l'Environnement, LCPME, UMR 7564 CNRS-Université Henri Poincaré Nancy 1, 405, rue de Vandoeuvre, 54600 Villers-les-Nancy, France*

ARTICLE INFO

ABSTRACT

The catalytic efficiency of iron (II, III) oxide to promote Fenton-like reaction was examined by employing Rhodamine B (RhB) as a model compound at neutral pH. Two types of iron (II, III) oxides were used as heterogeneous catalysts and characterized by XRD, Mössbauer spectroscopy, BET surface area, particle size and chemical analyses. The adsorption to the catalyst changed significantly with the pH value and the sorption isotherm was fitted using the Langmuir model for both solids. Both sorption and FTIR results indicated that surface complexation reaction may take place in the system. The variation of oxidation efficiency against H_2O_2 dosage and amount of exposed surface area per unit volume was evaluated and correlated with the adsorption behavior in the absence of oxidant. The occurrence of optimum amount of H_2O_2 or of exposed surface area for the effective degradation of RhB could be explained by the scavenging effect of hydroxyl radical by H_2O_2 or by iron oxide surface. Sorption and decolourization rate of RhB as well as H_2O_2 decomposition rate were found to be dependent on the surface characteristics of iron oxide. The kinetic oxidation experiments showed that structural Fe^{II} content strongly affects the reactivity towards H_2O_2 decomposition and therefore RhB decolourization. The site density and sorption ability of RhB on surface may also influence the oxidation performance in iron oxide/H_2O_2 system. The iron (II, III) oxide catalysts exhibited low iron leaching, good structural stability and no loss of performance in second reaction cycle. The sorption on the surface of iron oxide with catalytic oxidation using hydrogen peroxide would be an effective oxidation process for the contaminants.

1. Introduction

Chemical oxidation is a powerful method for the remediation of wastewater and contaminated groundwater. The hydroxyl radical ($^\bullet$OH), very reactive chemical species is generated in aqueous solution by well-known Fenton's reagent [1] (dissolved iron (II) + H_2O_2):

$$Fe^{II} + H_2O_2 \rightarrow Fe^{III} + HO^- + HO^\bullet \qquad (1)$$

Unlike the traditional Fenton's reagent where the pH values have to be lowered less than 4, the reaction between iron bearing minerals and hydrogen peroxide can effectively oxidize the organic molecules at circumneutral pH [2–5]. This process is called Fenton-like or modified Fenton which could avoid the initial acidification and may be costly and destructive for the *in situ* remediation of contaminated groundwater and soils. Several studies have investigated different iron oxide minerals for the Fenton-like reaction, such as ferrihydrite, hematite or goethite [2–5]. In heterogeneous

Fenton-like reaction, the decomposition rate of organic contaminants is slower than in traditional Fenton reaction using dissolved iron (II) at acidic pH. Recently, magnetite (Fe_3O_4) has been used in the investigation of heterogeneous catalytic oxidation [6–9]. The combination of oxidation states +2 and +3 in magnetite (giving an average oxidation state of +2.5) aids to increase decomposition of hydrogen peroxide, and enhance decomposition of organic contaminants [6–7].

Fenton-like process is a surface mineral-catalyzed system which can be explained by heterogeneous reactions occurring at the iron mineral surface [2–5]. The activity of the iron oxide used as catalyst depends on its characteristics such as crystallinity [10–12], surface area [10–13], iron content and/or iron oxidation state [8–9]. In the surface-catalyzed mechanism, the interactions of H_2O_2 with iron oxide surface lead to the formation of $HO^\bullet$ radicals which attack the pollutants in either sorbed or aqueous phases [2–5]. Watts et al. [3] reported that different mechanisms may occur on the surface at high H_2O_2 concentration and the sorption rate could be a controlling factor of the whole catalytic oxidation reaction. The catalytic activity for hydrogen peroxide decomposition and/or organic compound oxidation were widely investigated using Fe^{III}-bearing

---

* Corresponding author. Tel.: +33 3 83 68 52 42; fax: +33 3 83 27 54 44.
E-mail address: khalil.hanna@lcpme.cnrs-nancy.fr (K. Hanna).

minerals of different surface areas [2–5,10–13]. In these works, the authors proposed that the surface area of the iron oxide accounts for the difference in reaction activity and the decomposition rates by goethite, ferrihydrite, and hematite were all relatively similar when normalized to surface area. In this work, two mixed iron (II, III) oxides were selected to study the heterogeneous Fenton-like reaction. In addition to their structural Fe^{II} content, these oxides were chosen because of their different crystallinities and surface areas, which could affect their catalytic properties. The catalytic performance of iron (II, III) oxides was tested by taking into account their reactivity for oxidation of RhB used as a model compound. The Rhodamine B, xanthene dye, has become a common organic pollutant. It is a very stable non-volatile dye usually used in factories, has a comparatively high resistance to photo and oxidation degradation [14–15]. In this study, the decolourization rate of RhB solution in an iron oxide/H_2O_2 system was investigated at different amounts of H_2O_2 and exposed surface area per unit volume.

In order to evaluate the role of adsorption in the disappearance of pollutant in heterogeneous Fenton reaction, sorption experiments were conducted under various chemical conditions (sorbate concentration, pH, ionic strength). FTIR analysis was also investigated to describe the binding mechanism of RhB on the surface of iron oxide.

In fact, the deactivation of surface catalytic sites may be caused by the adsorption/oxidation process and/or solid-dissolution reaction in medium [10,16]. For this reason, XRD analysis was used to analyze the iron oxide structure before and after exposure to H_2O_2. In addition, the dissolution of iron form oxide structure was tested by chemical analyses and the presence of residue of organic compound on the oxide surface was tested by FTIR analysis.

2. Materials and methods

2.1. Chemicals

Rhodamine B (RhB) was procured from Sigma–Aldrich and used as such. Hydrogen peroxide (H_2O_2 35%, w/w) was obtained from Merck. Table 1 summarizes the properties of RhB. Two commercial Iron (II, III) oxides were used in this study. The first (called M1) was purchased from Aldrich Chemical Co. and the second (called M2) from Prolabo Co.

2.2. Solid characterization

In order to identify the crystal structure of minerals, samples of solids were analyzed by X-ray powder diffraction (XRD). The XRD data were collected with a D8 Bruker diffractometer, equipped

with a monochromator and a position-sensitive detector. The X-ray source was a Co anode ($\lambda = 0.17902$ nm). The diffractogram was recorded in the 3–64° 2θ range, with a 0.0359° step size and a collecting of 3 s per point.
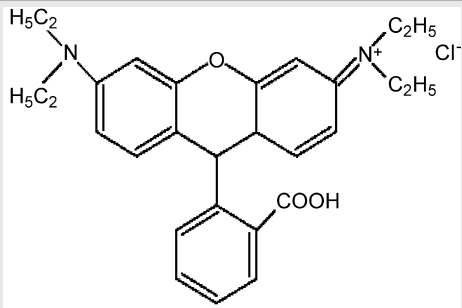
Reflection Mössbauer spectroscopy using MIMOS has been also employed to determine the oxidation state of iron and the iron mineralogy on the surface of iron oxides. In the present analysis, the MIMOS(II) source for the emission of characteristic g-rays was [57]Co which decays to the first excited state of [57]Fe. Details of procedure for MIMOS analysis are detailed in previous work [17].

The specific surface area of the iron oxides was determined by multipoint N_2–BET analysis using a Coulter (SA 3100) surface area analyzer. The particle size distribution was measured by a dynamic light-scattering method using Laser scattering particle size (HARIBA, LA 200). The site density or the concentration of the replaceable surface groups of magnetite was determined by measurement of the amount of fluoride adsorption on the surface [18]. Potentiometric titrations of the oxide were conducted in thermostated double walled pyrex cell at 293 K in 0.001, 0.01 and 0.1 M NaCl solutions according to the method of Parks and Bruyn [19]. The N_2 gas was constantly passed through the suspensions to bubble out the CO_2. The pH value of the suspension was adjusted with titrant solutions (HCl or NaOH) and recorded with the Orion pH meter model 710A having combination glass electrode. The blank titrations were also performed with similar solutions in the absence of the solid. Hence, the estimated pH of zero point of charge, pH_{zpc}, for both iron oxides is close to the value reported in the literature [20,21]. In addition, the electrophoretic mobility of the particles was measured with a Malvern Zetasizer (NanoZS) as a function of pH in 10 mM NaCl solution and then the zeta potential was calculated from the electrophoretic mobility [20,21]. The iso-electric point (IEP) of iron oxides are in agreement with the point of zero charge (PZC) determined by potentiometric titration (Table 2). The Fe^{II} content into oxide structure has been determined by chemical analysis after acid dissolution. The 6 N HCl ensures the dissolution of the iron oxide. Ferrous and total iron concentrations were determined using a modified 1,10-phenanthroline method [22]. The Fe^{II}/Fe^{III} ratio and total iron content (Fe_{tot}) of two oxides are reported in Table 2. All chemical analyses were performed in triplicate.

2.3. Sorption experiments

All equilibrium sorption experiments were conducted at 20 °C in the dark at neutral pH. The solid samples were mixed with variable solute concentrations. Results of adsorption kinetic experiments indicated that more than 98% of RhB sorption was achieved within 1 h. After equilibrium, the samples were filtered and ana-

Table 1
Some properties of the investigated dye.

Dye	Symbol	Mw (g mol^{-1})	pK_a	λ_{max} (nm)	ε (L mol^{-1} cm^{-1}) × 10^{-5}
Rhodamine B $C_{28}H_{31}N_2O_3Cl$	RhB	479.02	6.41	554	1.15 (pH 7)

Table 2
Physicochemical properties of two investigated oxides.

Solid	Fe_{tot} (wt.%)	Fe^{II}/Fe^{III} ratio	Mean particle diameter	SSA (m^2/g)	Site density ($\mu mol/m^2$)	PZC	IEP
M1	70 ± 2	0.24 ± 0.2	<50 nm	40 ± 3	1.7 ± 0.1	7.8	8.0
M2	70 ± 2	0.43 ± 0.2	<5 μm	2.4 ± 0.2	3.6 ± 0.2	7.4	7.2

lyzed by UV–visible spectroscopy and sorbed concentrations were calculated by difference according to:

$$q_e = \frac{(C_i - C_e)V}{M_s A} \qquad (2)$$

Where q_e (mmol/m^2) is the sorbed concentration, C_e (mmol/L) is the equilibrium concentration at the end of the experiment, C_i (mmol/L) is the initial aqueous phase concentration, V (L) is the volume of solution, M_s (g) is the mass of solid sorbent, and A (m^2/g) is the sorbent specific surface area. The sorption equilibrium experiments were performed in triplicate. The standard deviation of the three replicates was less than 4%. Adsorption experiments versus pH were performed with a single initial solute concentration in a 200 mL closed reaction vessel at a constant temperature and in the dark. The pH was controlled by adding HCl or NaOH to the stock solid suspensions. Ionic strength effect on RhB sorption was conducted using NaCl at various molar concentrations (1–100 mM) at fixed pH. The RhB concentration in solution can be determined by measuring the absorbance using a UV–Vis spectrophotometer (PerkinElmer), using a 1 cm quartz cell. Calibration curves were obtained by using the standard RhB solutions with known concentrations at various pH (3–10).

A Fourier transform infrared spectrometer PerkinElmer 2000, equipped with a KBr beam splitter and a MCT detector, was also used for sorption characterization by vibrational spectroscopy. The spectral resolution and the total acquisition time were respectively 4 cm^{-1} and 5 min. FTIR spectra in diffuse reflectance mode were collected using Harrick DRA-2CI equipment. To perform the analysis, the solid samples were first diluted in a KBr matrix (5 wt.%). The samples were mixed very gently with KBr in an agate mortar; so that these mixtures were not subjected to any elevated pressures. The reflectances (R_s) of the sample and (R_r) of pure KBr, used as a non-absorbing reference powder, were measured under the same conditions. The iron hydroxide reflectance is defined as $R = R_s/R_r$. The spectra is shown in pseudo-absorbance ($-\log R$) mode.

2.4. Oxidation experiments of RhB

The dye and the mixed oxide were stirred for 90 min to ensure the adsorption equilibrium. After this period, 3 mL aliquot was withdrawn to determine the concentration C_0 and then the oxidant was added to the suspension. The solution pH was adjusted to 7 and kept within 0.1 pH units of this value with diluted solutions of HClO$_4$ and NaOH during the experiments.

During all the oxidation reactions, 3 mL aliquots were withdrawn at selected time intervals, filtered and analyzed. When H$_2$O$_2$ was used as an oxidant in the absence of catalyst, oxidation of the starting compound was always very slow. The decolourization experiments were monitored by UV–Vis spectrophotometer. All experimental runs were performed within a temperature of 20 °C in the absence of light. Each experiment was performed in triplicates, all results were expressed as a mean value of the 3 experiments.

In addition, the Fe leaching behavior from solids or eventual oxide dissolution was evaluated along the experiments under different conditions. ICP/AES (detection limit 1.5 μg/L) was used to monitor the Fe concentration in reaction solution (with and without H$_2$O$_2$) versus time.

H$_2$O$_2$ was measured using the modified *N,N*-diethyl-*p*-phenylenediamine DPD method [23]. This method measures H$_2$O$_2$

concentrations over the range 5–50 μmol L^{-1}. Because the H$_2$O$_2$ concentrations in the experimental reactors were above this range, each sample was diluted. 0.5 mL of phosphate buffer (pH 6.0) and 5 mL aliquot of diluted sample was mixed in the reaction vial. An aliquot of 50 μL of DPD reagent (3.8×10^{-2} M in 0.1 M H$_2$SO$_4$) followed by 50 μL (100 units mL^{-1}) of horseradish peroxidase were then added to reaction vial. The cell was manually shaken for a minute for color development. Absorbance readings were taken at 551 nm using a UV–Vis spectrophotometer.

3. Results and discussion

3.1. Characterization of solid samples

The diffractograms of both iron oxides are shown in Fig. 1. Five diffraction peaks at 2θ = 21.2°, 35°, 41.2°, 50.4° and 62.8° are shown in the XRD diffractogram (Fig. 1), which could be assigned to Fe$_3$O$_4$, magnetite [24]. The *d*-space values of these main peaks were 2.53, 2.96, 2.09, 4.85 and 1.71 Å which may correspond to the more intense lines 311, 220, 400, 111 and 422, respectively of magnetite [24]. Therefore, the spectra of solid M2 may correspond to that of the magnetite [24], which can be confirmed by Mössbauer analysis. It should be noted that the XRD pattern of M1 shows the same peaks which are less intense. The broad nature and low intensity of the peaks in the spectra of M1 can result from nanosized particles (Table 2) which may exhibit a poor crystallinity [24,25]. Some surface properties of two iron oxides are reported in Table 2.

3.2. Sorption of RhB on M1 and M2

Sorption isotherms were determined to assess RhB distribution between solid and aqueous phases and to investigate the effect of contaminant sorption on the catalytic oxidation (Fig. 2). The experimental isotherm data were fitted to the equations of Langmuir, Freundlich and Tempkin by applying linear regression analysis. One way to assess the goodness of fit of experimental isotherm data to these equations is to perform an analysis of variance (ANOVA) with error calculation. On the basis of the statistical analysis, the curves were shown a best fit with Langmuir model for both solids. The
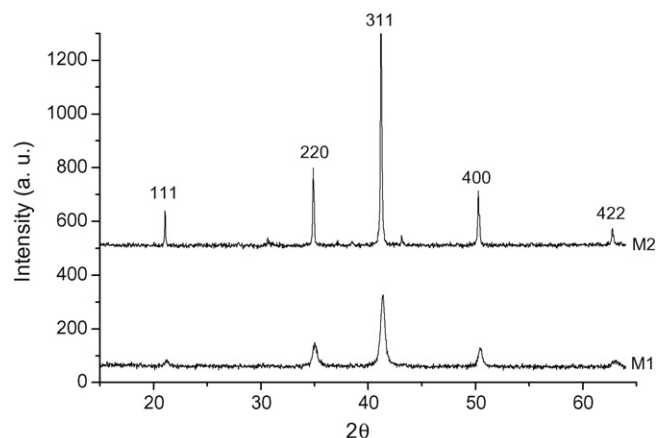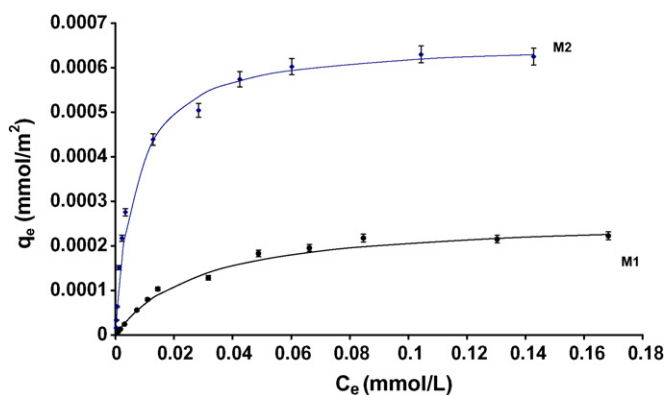

Fig. 1. XRD of M1 and M2.

Fig. 2. Sorption isotherms of RhB at pH 7.

linear form of the Langmuir equation is given by:

$$\frac{C_e}{q_e} = \frac{1}{K_L} + \frac{a_L}{K_L}C_e \qquad (3)$$

where a_L (L/mmol) and K_L (L/m^2) are the Langmuir isotherm constants. Langmuir monolayer sorption capacity (mmol/m^2) is numerically equal to K_L/a_L. An increasing RhB concentration showed a progressive saturation of the surface sites. On surface area basis, the sorption intrinsic capacity of M2 is higher than of M1. The Langmuir isotherm constants obtained by plotting C_e/q_e against C_e are $a_L = 36$ L/mmol and $K_L = 0.0095$ L/m^2 for M1, $a_L = 153.5$ L/mmol and $K_L = 0.101$ L/m^2 for M2.

In general, the sorption behavior versus pH could be attributed to a combination of pH-dependent speciation of sorbate, surface charge characteristics of the mineral oxides. For M1, RhB sorption onto oxides slightly increased with increasing pH from 3 to 7, while it decreased with increasing pH for solid M2 (Fig. 3a). No electrostatic interactions between the carboxyl groups in the dye (pK_a 6.41) and positively charged iron sites are expected. Above pH 7, the sorption stayed almost constant for both solids, even though both the sorbate and the surface sorbent were negatively charged. The surface charge of solids deduced from the zeta potential curve varies from positive to negative, according to the point of zero charge due to deprotonation of surface hydroxyls (Fig. 3b). Therefore, no electrostatic repulsions between the increasingly negative surface charge and the deprotonated carboxylic group of RhB are expected. This data was not consistent with some studies where the adsorption envelope of organic acids bound to iron oxide typically showed maximum adsorption at a pH near the pK_a [26,27 and refs cited in 27].

Effect of ionic strength on RhB sorption was investigated by conducting sorption equilibrium experiment at different NaCl concentrations (from 1 to 100 mM of NaCl) at 20 °C. Less than 5% of sorption was decreased by the introduction of NaCl ions, implying that the ionic strength did not affect the sorption behavior to iron oxide surface. Because Cl$^-$ can associate with the iron oxide surface as outer-sphere complexes and RhB sorption was independent on ionic strength including NaCl, it can be concluded that sorption mechanism of RhB on oxide surfaces was stronger than non-specific electrostatic interactions or outer-sphere complexes. In accord with all data listed above, the surface complexation mechanism was expected for RhB sorption on both iron oxides. By analogous structure with some carboxylate compounds, the adsorption of RhB expected to occur via the carboxylic group of RhB through the formation of a mononuclear monodentate complex with iron surface sites [27 and refs cited in it]. The IR spectra of RhB equilibrated with iron oxide were recorded at wavelength range 2000–1000 cm^{-1} at two pH values 3 and 7 (Fig. 4). The peaks at 1592 cm^{-1} and at around 1500 cm^{-1} correspond to aromatic ring vibrations, while
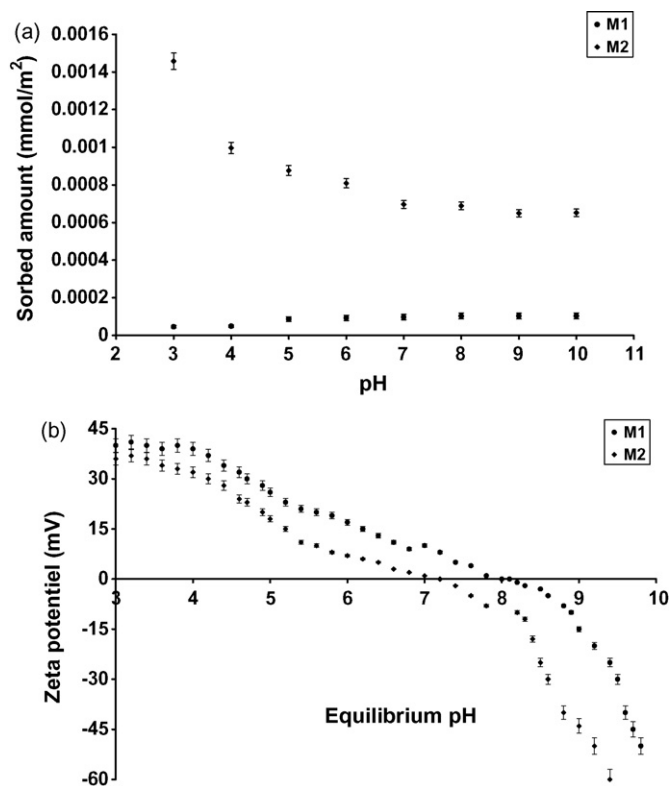

Fig. 3. RhB sorption (a) and Zeta potential measurements (b) versus pH of both iron oxides.

the 1345 cm^{-1} peak attributes to C-aryl bond vibration. The peak at 1648 cm^{-1} is caused by vibrations of the C—N bond [14]. The C=O is associated with the band at 1694 cm^{-1} and the C—OH bond with the group of bands in the range 1088–1300 cm^{-1} [28]. In fact, it was not possible from the FTIR results to determine the preferred binding site for RhB sorption. The IR spectrum of RhB sorbed onto iron oxide surface is almost unchanged with the increase in pH (3 to 7). The overall intensity of adsorbate spectra depended on solid type and pH value, corroborating the batch sorption data. No significant difference of RhB sorbed spectrum was observed for M1 or M2, so the same type of surface complex may occur on the surface of both iron oxides. So, the sorption mechanism of RhB on both oxides seems to be identical at both the studied
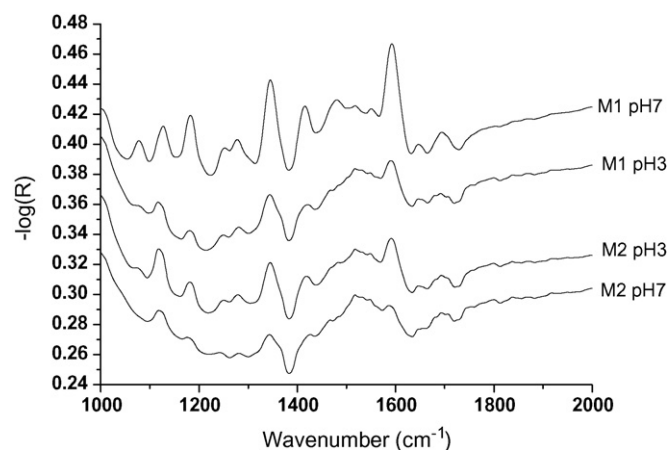

Fig. 4. Infrared spectra of solid samples equilibrated in the dark in RhB (5 mM) at two pH values.

pH values even though the sorption edges did not reveal a similar trend.

3.3. Effect of H_2O_2 dose on decolourization rate of RhB solution at neutral pH

The oxidation kinetics was studied to quantitatively characterize the decolourization at neutral pH in the presence of 2 g/L of iron oxide. Preliminary test showed that no significant photochemical reaction of RhB was observed by natural light under our experimental conditions.

Hydroxyl radical can be generated by the reaction between hydrogen peroxide and iron surface leading to a decolourization of RhB solution. The degradation of organic compounds by HO$^\bullet$ is typically described as a second-order reaction:

$$\frac{dC}{dt} = -kC[\text{HO}^\bullet] \tag{4}$$

where C and $[\text{HO}^\bullet]$ are concentrations of RhB in water and hydroxyl radical, respectively, k is the second-order rate constant, and t is the reaction time. By assuming that HO$^\bullet$ instantaneous concentration is constant, the kinetics of decolourization of RhB in water can be described according to the pseudo-first-order equation as given below:
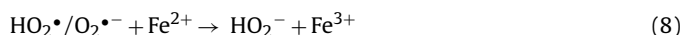
$$C_t = C_0 \exp(-k_{app}t) \tag{5}$$

where C_0 is the initial concentration of RhB and k_{app} is the pseudo-first-order apparent rate constant (min^{-1}). The k_{app} constants were obtained from the slopes of the straight lines by plotting $-\ln(C_t/C_0)$ as a function of time t, through regression.

The kinetic constants rate k_{app} were determined at different H_2O_2 concentrations (Fig. 5). At all ranges of H_2O_2/Fe ratio, M2 exhibits better oxidation capacity than M1. Since the decolourization of RhB solution is directly related to the concentration of the hydroxyl radicals produced by the catalytic decomposition of hydrogen peroxide, more RhB decomposition is expected when hydrogen peroxide dosage increases. However, a decrease in the values of k_{app} was observed at a much higher H_2O_2 concentration (Fig. 5). The occurrence of this optimum H_2O_2 concentration for the effective degradation of the dye could be explained by the scavenging effect of hydroxyl radicals by hydrogen peroxide. A similar observation was noted earlier for the degradation of organic compounds by Fenton-like reactions using goethite as catalyst [29]. At low H_2O_2 concentration, the HO$^\bullet$ radicals preferentially attack the substrate molecules, whereas at higher H_2O_2 concentration, there is a competitive reaction between the substrate and H_2O_2. The $^\bullet$OH radical may react with hydrogen peroxide producing super-

oxide/hydroperoxy radicals according to Eq. (6):

$$^\bullet\text{OH} + H_2O_2 \rightarrow \text{HO}_2{}^\bullet/\text{O}_2{}^{\bullet-} + H_2O \tag{6}$$
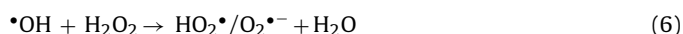
Buxton et al. [30] have determined the reaction rate of H_2O_2 with hydroxyl radical ($k = 2.7 \times 10^7 \, \text{M}^{-1} \, \text{s}^{-1}$). Because the p$K_a$ of HO$_2{}^\bullet$/O$_2{}^{\bullet-}$ is 4.8, generation of hydroperoxide anion HO$_2{}^\bullet$ may be neglected at neutral pH. The generated radicals O$_2{}^{\bullet-}$ are much less reactive and do not contribute to any oxidation of RhB [2]. O$_2{}^{\bullet-}$ plays an important role in the redox cycle of Fe^{2+} and Fe^{3+} in aqueous phase and generates oxygen as a byproduct but the interactions of superoxide/hydroperoxy radicals with the iron mineral surface are not yet well argued:

$$\text{O}_2{}^{\bullet-} + Fe^{3+} \rightarrow \text{O}_2 + Fe^{2+} \tag{7}$$

$$\text{HO}_2{}^\bullet/\text{O}_2{}^{\bullet-} + Fe^{2+} \rightarrow \text{HO}_2{}^- + Fe^{3+} \tag{8}$$

3.4. H_2O_2 decomposition and RhB removal versus exposed surface area per unit volume

The H_2O_2 decomposition versus time at various surface area for M1 (A) and M2 (B) is presented in Fig. 6. Good linear plot obtained with the expressions of $\ln([H_2O_2]/[H_2O_2]_0)$ as a function of the reaction time, indicates that the H_2O_2 decomposition is the first-order reaction.

$$\frac{d[H_2O_2]}{dt} = -k_{app}[H_2O_2] \tag{9}$$

where $k_{app} = k[\text{SSA}]$.

[SSA] means the amount of specific surface area per unit volume (m^2/L). The H_2O_2 decomposition rate k_{app} (min^{-1}) was plotted as a function of [SSA] (Fig. 7). The good linear relationship ($R^2 = 0.99$) between the rate constant and [SSA] indicates that the H_2O_2 decomposition is the first-order reaction with oxide surface area. The results clearly indicate that this is the surface reaction because the increase of surface area provides more active sites for catalytic oxidation. The second-order rate constant (k) obtained from the plot of observed first-order rate constant for H_2O_2 decomposition versus [SSA] is $3.10^{-4} \, \text{min}^{-1} \, (\text{m}^2/\text{L})^{-1}$ for M2 and $8.10^{-5} \, \text{min}^{-1} \, (\text{m}^2/\text{L})^{-1}$ for M1. The H_2O_2 decomposition versus time at 1 g/L for both oxides is shown in Fig. 6C. The H_2O_2 decomposition rate was higher for M2 than M1 based on surface area basis, while the trend is opposite based on mass basis.

The decolourization of RhB solution was also investigated at various [SSA]. The good linear plot obtained with the expressions of $\ln([\text{RhB}]/[\text{RhB}]_0)$ as a function of the reaction time, allows determining the first-order kinetic constant:

$$\frac{d[\text{RhB}]}{dt} = -k_{app}[\text{RhB}] \tag{10}$$

A plot of observed first-order rate constant k_{app} (min^{-1}) for dye removal as a function of [SSA] is shown in Fig. 8. In contrast with the result of Fig. 7, the RhB removal was not proportional to the oxide surface area. The observed first-order rate constant for dye removal firstly increased with increasing [SSA] and then reduced. This phenomenon can be explained from the assumption that OH radical generated by the reaction between hydrogen peroxide and iron oxide is scavenged by iron surface. Miller and Valentine [11] reported that OH radical is very reactive with natural iron oxide-coated sand ($k = 8 \times 10^{11} \, (\text{g/mL})^{-1} \, \text{s}^{-1}$). Regarding this data (Fig. 8), M2 exhibits better oxidation performance than M1 at full range of studied [SSA] (3–40 m^2/L). Furthermore, M$_1$ seems to be a more radical scavenger than M2, where the SSA optimum occurred at about 17 m^2/L for M1 and at 32 m^2/L for M2.

Oxidation efficiency was assessed by the following equation:

$$E\left(\frac{\text{mole}}{\text{mole}}\right) = \frac{\Delta[\text{RhB}]}{\Delta[H_2O_2]} \tag{11}$$

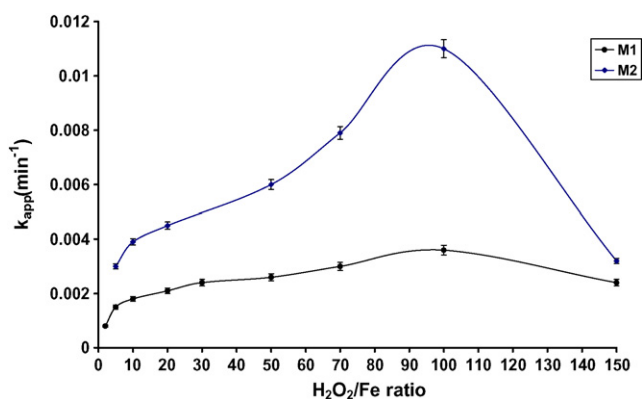**Fig. 5.** Effect of H_2O_2/Fe ratio on the decolourization kinetic constant of RhB. H_2O_2/Fe (molar ratio) = 5–150, [RhB] = 5 mg/L, [Iron (II, III) oxide] = 2 g/L, 20 °C, pH 7.
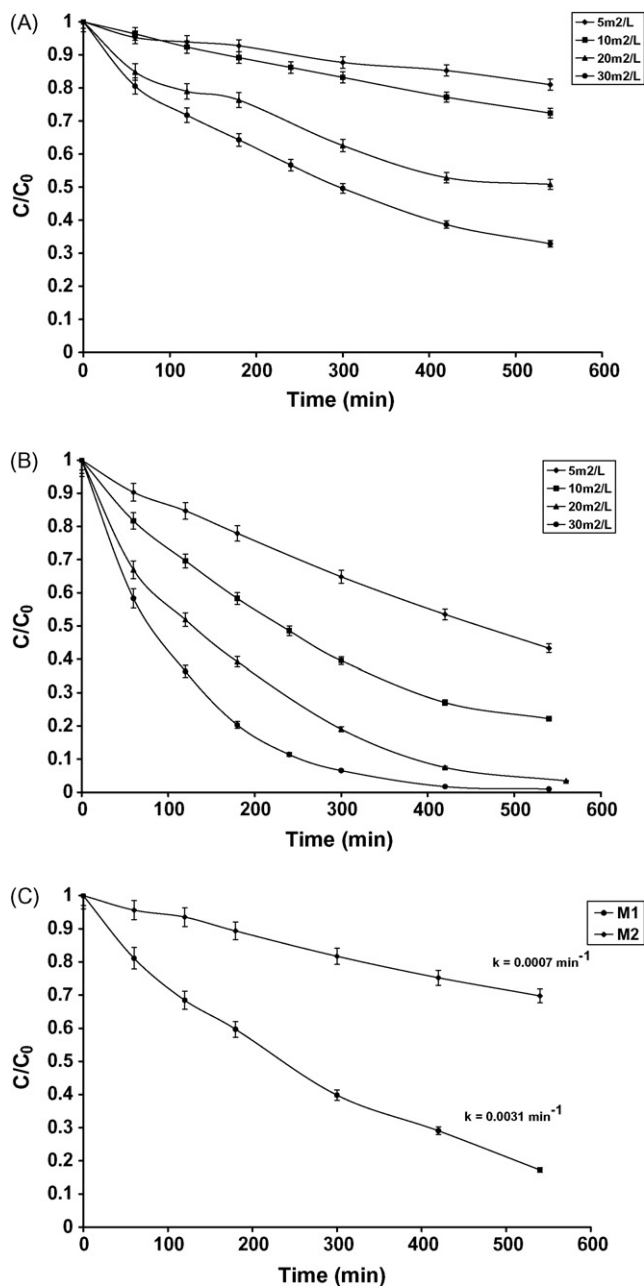
(A)

(B)

(C)

Fig. 6. H_2O_2 decomposition at various [SSA] of M1 (A) and M2 (B) and at 1 g/L of both solids (C). $[H_2O_2] = 1$ mM, 20 °C, pH 7.

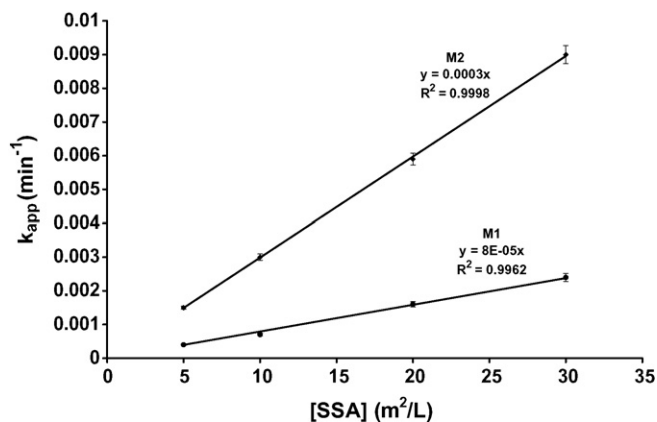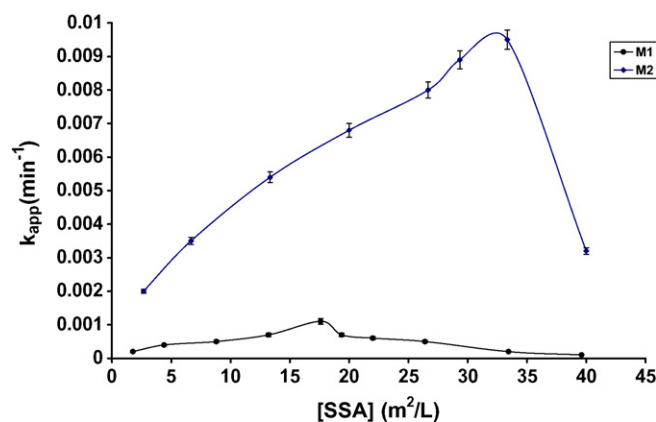**Fig. 7.** H_2O_2 decomposition rate versus [SSA]. $[H_2O_2] = 1$ mM, 20 °C, pH 7.

Fig. 8. Effect of [SSA] on the decolourization kinetic constant of RhB. $[H_2O_2] = 150$ mM, 20 °C, pH 7.

where E(mole/mole) is the stoichiometry efficiency while Δ[RhB] and $\Delta[H_2O_2]$ represent the variation in molar concentration of RhB and H_2O_2 as a function of [SSA]. A high E value means a high reaction yield between RhB and hydroxyl radicals. Fig. 9 shows that E for dye removal is inversely proportional to the amount of oxide surface area, corroborating that iron surface can act as an OH radical scavenger. A sharp decrease in oxidation efficiency (E) was observed for M1, while a first rise in the E value before a slow decrease was observed for M2. On the basis of this data, M1 seems to be less reactive and more HO• scavenged in comparison with M2. This difference in oxidation efficiency might be due to difference in mineral structural properties (crystallography, Fe^{II} content). Valentine and Wang [10] reported that an amorphous iron oxide has more vacant Fe sites and OH groups able to scavenge hydroxyl radicals than crystallized iron oxides. Valentine and Wang [10] and Huang et al. [12] showed that the hydrogen peroxide decomposition rate was the highest for ferrihydrite, less for semicrystalline oxide, and much less for goethite or hematite (high crystallized oxide). However, they also affirmed that the catalytic activity for organic compound oxidation exhibited a converse series for these iron oxides, corresponding to the inverse sequence of specific surface area. Indeed, an amorphous iron oxide with high surface area may improve the decomposition of H_2O_2 via non-radical pathway [4,5]. However, it should be noted that the reaction of H_2O_2 decomposition would not be expected to yield a simple dependence of HO• generation rate.

In the present study, the H_2O_2 decomposition rate was higher for M2 than for M1 when normalized to the oxide surface area. However, the trend is inversed when based on oxide mass basis
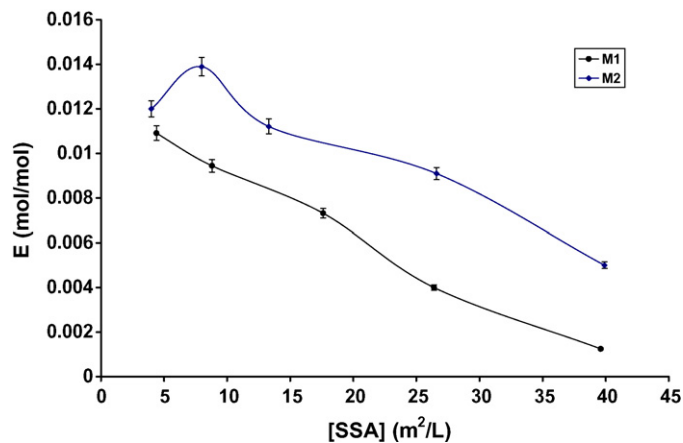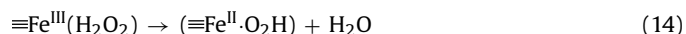

Fig. 9. Oxidation efficiency (E) versus [SSA].

($M1 (40 \, m^2/g) > M2 (2.4 \, m^2/g)$). On the basis of both mass and surface area, the dye decolourization rate was higher for M2 (high crystallinity, $2.4 \, m^2/g$) than for M1 (low crystallinity, $40 \, m^2/g$). This discrepancy may be probably due to the fact that the surface reactivity of the mixed oxides depended on surface properties such as structural Fe^{II} content. Firstly, Fe^{II} plays an important role for the initiation of the Fenton reaction according to the classical Haber–Weiss mechanism and therefore the enhancement of the production rate of $^{\bullet}OH$ [2,31]. Heterogeneous reactions analogous to the solution phase reactions were used to explain the interactions between oxidant and iron surface:

$$\equiv Fe^{II} + H_2O_2 \rightarrow \ \equiv Fe^{III} + HO^- + HO^{\bullet} \tag{12}$$

$$\equiv Fe^{III} + H_2O_2 \rightarrow \ \equiv Fe^{III}(H_2O_2) \tag{13}$$

$$\equiv Fe^{III}(H_2O_2) \rightarrow (\equiv Fe^{II} \cdot O_2H) + H_2O \tag{14}$$

$$(\equiv Fe^{II} \cdot O_2H) \rightarrow \ \equiv Fe^{II} + HO_2^{\bullet} \tag{15}$$

In mineral catalyzed reaction, the dominant reaction is first a chain of reactions occurring on the mineral surface. If only Fe^{III} is originally present, Fe^{II} is slowly generated by reactions (13)–(15) initiating oxidation reaction (12). In the case of mixed Fe^{II}–Fe^{III}-bearing mineral, reactions involving both Fe^{II} and Fe^{III} may occur. Therefore, the presence of iron (II) in the Fe-bearing minerals can enhance the production rate of $HO^{\bullet}$ [2,31–33].

3.5. Structural and catalytic stabilities

The action of H_2O_2 on the oxide surface can transform the oxide particles into a only Fe^{III}-bearing mineral or into a amorphous iron oxide which may be less stable and more soluble. This mineralogical transformation may lead to a substantial change in the surface characteristics of the mineral, causing a different kinetic behavior and decomposition rate for H_2O_2. The very low dissolved iron concentration measured in all our studied systems did not expect the formation of more soluble iron oxide. Furthermore, chemical analysis, XRD analysis of both oxides was conducted before and after exposure to H_2O_2. The chemical analyses of the solid after reaction revealed no significant change in the total Fe loading. In addition, XRD patterns recorded at the end of oxidation reaction was found to be similar to that recorded before reaction (Fig. 1).

The reusability of the solids has been evaluated under identical oxidation conditions as explained in our previous work [9]. At the end of the oxidation process, the solid is easily removed from the reactor, dried in the glovebox under N_2 and stored at ambient temperature. The FTIR spectrum of the recovered solid was recorded at wavelength range $2000–1000 \, cm^{-1}$. It is noted that the absorption peaks for sorbed RhB in the range $1000–1700 \, cm^{-1}$ (Fig. 4) almost disappeared and there is no residue of organic compounds on the surface of the solid. The H_2O_2 decomposition and RhB decolourization on the recovered catalyst were then investigated as for previous experiments and showed a slight difference with the first oxidation cycle. The excellent stability of the catalytic activity could be attributed to the low loss of iron content during oxidation cycles and to the structural stability of the solid.

4. Conclusion

The removal rate of organic compound by Fenton-like oxidation firstly increased with the dosage of H_2O_2 or with the amount of exposed surface area, reached an optimum value and then decreased. The occurrence of these optimum values for the effective degradation of the dye could be explained by the scavenging and parasite reactions with (i) H_2O_2 or (ii) iron oxide surface. Only heterogeneous Fenton reaction happened for the decolourization of Rhodamine B (RhB) because Fe leaching from the oxide surface

is negligible at neutral pH. M2 exhibits important intrinsic reactivity for RhB decolourization or H_2O_2 decomposition. On surface area basis, RhB sorption and H_2O_2 decomposition rates on the surface of oxide were higher for M2 (high crystallinity and Fe^{II}/Fe^{III} ratio) than for M1 (low crystallinity and Fe^{II}/Fe^{III} ratio). M2 exhibits better oxidation efficiency for dye removal than M1 on the basis of both mass and surface area. The decomposition of RhB on M2 is higher than M1 even though the sorption mechanism of RhB on the surface of both oxides revealed a similar trend. The site density and sorption ability of RhB on catalyst surface may also influence the oxidation performance in iron oxide/H_2O_2 system. The iron oxide catalysts exhibited low iron leaching, good structural stability and no loss of performance in second reaction cycle. The sorption on the surface of iron oxide with catalytic oxidation using hydrogen peroxide would be an effective oxidation process for the contaminants.

References

[1] H.J.H. Fenton, Oxidation of tartaric acid in presence of iron, J. Chem. Soc. (Br.) 65 (1894) 899–910.
[2] S.S. Lin, M.D. Gurol, Catalytic decomposition of hydrogen peroxide on iron oxide: kinetics, mechanism, and implications, Environ. Sci. Technol. 32 (1998) 1417–1423.
[3] R.J. Watts, M.K. Foget, S.H. Kong, A.L. Teel, Hydrogen peroxide decomposition in model subsurface systems, J. Hazard. Mater. 69 (1999) 229–243.
[4] W.P. Kwan, B.M. Voelker, Decomposition of hydrogen peroxide and organic compounds in the presence of dissolved iron and ferrihydrite, Environ. Sci. Technol. 36 (2002) 1467–1476.
[5] W.P. Kwan, B.M. Voelker, Rates of hydroxyl radical generation and organic compound oxidation in mineral-catalyzed Fenton-like systems, Environ. Sci. Technol. 37 (2003) 1150–1158.
[6] S.H. Kong, R.J. Watts, J.-H. Choi, Treatment of petroleum-contaminated soil using iron mineral catalyzed hydrogen peroxide, Chemosphere 37 (1998) 1473–1482.
[7] R.J. Watts, M.D. Udell, S.G. Kong, S.W. Leung, Fenton-like soil remediation catalysis by naturally occurring iron minerals, Environ. Eng. Sci. 16 (1999) 93–103.
[8] R. Matta, K. Hanna, S. Chiron, Fenton-like oxidation of 2,4,6-trinitrotoluene using different iron mineral, Sci. Total Environ. 385 (2007) 242–251.
[9] K. Hanna, T. Kone, G. Medhagi, Synthesis of the mixed oxides of iron and quartz and their catalytic activities for the Fenton-like oxidation, Catal. Commun. 9 (2008) 955–959.
[10] R.L. Valentine, H.C.A. Wang, Iron oxide surface catalyzed oxidation of quinoline by hydrogen peroxide, J. Environ. Eng. 124 (1998) 31–38.
[11] C.M. Miller, R.L. Valentine, Mechanistic studies of surface catalyzed H_2O_2 decomposition and contaminant degradation in the presence of sand, Water Res. 33 (1999) 2805–2816.
[12] H.H. Huang, M.C. Lu, J.N. Chen, Catalytic decomposition of hydrogen peroxide and 2-chlorophoen with iron oxides, Water Res. 35 (2001) 2291–2299.
[13] W.P. Kwan, B.M. Voelker, Influence of electrostatics on the oxidation rates of organic compounds in heterogeneous Fenton systems, Environ. Sci. Technol. 38 (2004) 3425–3431.
[14] A.K. Mittal, Venkobachar, Uptake of cationic dyes by sulfonated coal: sorption mechanism, Ind. Eng. Chem. Res. 35 (1996) 1472–1474.
[15] Z. Ai, L. Lu, J. Li, L. Zhang, J. Qiu, M. Wu, Fe/@Fe_2O_3 coreshell nanowires as iron reagent.1.Efficient degradation of Rhodamine B by a novel sono-Fenton process, Phys. Chem. C. 111 (2007) 4087–4093.
[16] J. Barrault, M. Abdellaoui, C. Bouchoule, A. Majeste, J.M. Tatibouet, A. Louloudi, N. Papayannakos, N.H. Gangas, Catalytic wet peroxide oxidation over mixed (Al–Fe) pillared clays, Appl. Catal. B Environ. 27 (2000) 225–230.
[17] V. Khare, M. Mullet, K. Hanna, M. Blumers, M. Abdelmoula, G. Klingelhöfer, Comparative studies of ferric green rust and ferrihydrite coated sand: role of synthesis routes, Solid State Sci. 10 (2008) 1342–1351.
[18] L. Sigg, W. Stumm, The interactions of anions and weak acids with the hydrous goethite surface, Colloids Surf. 2 (1981) 101–117.
[19] G.A. Parks, P.L.J. Bruyn, The zero point charge of oxides, Phys. Chem. 66 (1962) 967–973.
[20] T.J. Daou, S. Begin-Colin, J.M. Greneche, F. Thomas, A. Derory, P. Bernhardt, P. Legare, G. Pourroy, Phosphate adsorption properties of magnetite-based nanoparticles, Chem. Mater. 19 (2007) 4494–4505.
[21] N.N. Marmier, A. Delisée, F. Fromage, Surface complexation modeling of Yb(III), Ni(II), and Cs(I) sorption on magnetite, J. Colloid Interface Sci. 211 (1999) 54–60.

[22] H. Tamura, K. Goto, T. Yotsuyanagi, M. Nagayama, Spectroscopic determination of iron with 1,10-phenantroline in the presence of large amounts of iron, Talanta 21 (1974) 314–318.

[23] H. Bader, V. Sturzenegger, J. Hoigné, Photometric method for the determination of low concentrations of hydrogen peroxide by the peroxidase catalyzed oxidation of N,N-diethyl-p-phenylenediamine (DPD), Water Res. 22 (1988) 1109–1115.

[24] U. Schwertmann, R.M. Cornell, Iron oxides in the laboratory: preparation and characterization, Wiley-VCH, New York, 2000.

[25] S.H. Xuan, L.Y. Hao, W.Q. Jiang, X.L. Gong, Y. Hu, Z.Y. Chen, Preparation of water-soluble magnetite nanocrystals through hydrothermal approach, J. Magn. Magn. Mater. 308 (2007) 210–213.

[26] K. Hanna, Sorption of two aromatic acids onto iron oxides: experimental study and modeling, J. Colloid Interface Sci. 309 (2007) 419–428.

[27] K. Hanna, C. Carteret, Sorption of 1-hydroxy-2-naphthoic acid to goethite, lepidocrocite and ferrihydrite: batch experiments and infrared study, Chemosphere 70 (2007) 178–186.

[28] K. Nakomoto, Infrared and Raman spectra of inorganic and coordination compounds, 4th ed., J. Wiley Sons, New York, 1986.

[29] J.J. Wu, M. Muruganandham, J.S. Yang, S.S. Lin, Oxidation of DMSO on goethite catalyst in the presence of H_2O_2 at neutral pH, Catal. Commun. 7 (2006) 901–906.

[30] G.V. Buxton, C.L. Greenstock, W.P. Helman, A.B. Ross, Critical review of rate constants for reactions of hydrated electrons, hydrogen atoms and hydroxyl radicals ($OH^{\bullet}/O^{\bullet -}$) in aqueous solution, J. Phys. Chem. 17 (1988) 513–886.

[31] F. Haber, J. Weiss, The catalytic decomposition of hydrogen peroxide by ferrous salts, Proc. R. Soc. Lond. Ser. A 147 (1934) 332–351.

[32] R. Matta, K. Hanna, S. Chiron, Oxidation of phenol by green rust and hydrogen peroxide at neutral pH, Sep. Purif. Technol. 61 (2008) 442–446.

[33] R. Matta, K. Hanna, T. Kone, S. Chiron, Oxidation of 2,4,6-trinitrotoluene in the presence of different iron-bearing minerals at neutral pH, Chem. Eng. J. 144 (2008) 453–458.